Journal of Biomaterials Applications

Photothermal stress triggered by near infrared-irradiated carbon nanotubes promotes bone deposition in rat calvarial defects

Journal:	*Journal of Biomaterials Applications*
Manuscript ID:	Draft
Manuscript Type:	Original Manuscript
Date Submitted by the Author:	n/a
Complete List of Authors:	Yanagi, Tsukasa; Fukuoka Dental College, Department of Oral Rehabilitation Kajiya, Hiroshi; Fukuoka Dental College, Department of Physiological Science and Molecular Biology Kawaguchi, Minoru; Fukuoka Dental College, Department of Dental Engineering Kido, Hirofumi; Fukuoka Dental College, Department of Oral Rehabilitation Fukusima, Tadao; Fukuoka Dental College, Center for Regenerative Medicine
Keywords:	Photothermal stress stimulation, DNA/protamine scaffold, bone deposition, preosteoblasts, osteogenesis
Abstract:	The bone regenerative healing process is often prolonged, with a high risk of infection particularly in elderly and diseased patients. A reduction in healing process time usually requires mechanical stress devices, chemical cues, or laser/thermal therapies. Although these approaches have been used extensively for the reduction of bone healing time, the exact mechanisms involved in thermal stress-induced bone regeneration remain unclear. In this study, we investigated the effect of optimal hyperthermia on rat calvarial defects in vivo and on osteogenesis in vitro. Photothermal stress (PTS) stimulation was carried out using a new photothermal device, composed of an alginate gel including incarbon nanotubes (CNT) and their irradiator with near-infrared (NIR) light. PTS (15 min at 42°C, every day), trigged by NIR-induced CNT, promoted bone deposition in critical-sized calvarial defects compared with non-thermal stress controls. We recently reported that our novel DNA/protamine (D/P) complex scaffold induces bone regeneration in calvarial defects. In this study, PTS upregulated bone deposition in D/P-engrafted calvarial defects. Furthermore, PTS significantly induced expression of osteogenic related genes in a time-depended manner, including alkaline phosphatase, osterix and osteocalcin. This was observed in DP-cells, which were expanded from regenerated tissue engrafted into the D/P scaffold, as well as in human MG63 preosteoblasts. In summary, this novel CNT-based PTS approach upregulated expression of osteogenic-related genes in preosteoblasts, resulting in promotion of mineral deposition for enhanced bone repair.

Photothermal stress triggered by near infrared-irradiated carbon nanotubes promotes bone deposition in rat calvarial defects

Abstract

The bone regenerative healing process is often prolonged, with a high risk of infection particularly in elderly and diseased patients. A reduction in healing process time usually requires mechanical stress devices, chemical cues, or laser/thermal therapies. Although these approaches have been used extensively for the reduction of bone healing time, the exact mechanisms involved in thermal stress-induced bone regeneration remain unclear. In this study, we investigated the effect of optimal hyperthermia on rat calvarial defects *in vivo* and on osteogenesis *in vitro*. Photothermal stress (PTS) stimulation was carried out using a new photothermal device, composed of an alginate gel including incarbon nanotubes (CNT) and their irradiator with near-infrared (NIR) light. PTS (15 min at 42°C, every day), trigged by NIR-induced CNT, promoted bone deposition in critical-sized calvarial defects compared with non-thermal stress controls. We recently reported that our novel DNA/protamine (D/P) complex scaffold induces bone regeneration in calvarial defects. In this study, PTS upregulated bone deposition in D/P-engrafted calvarial defects. Furthermore, PTS significantly induced expression of osteogenic related genes in a time-depended manner, including alkaline phosphatase, osterix and osteocalcin. This was observed in DP-cells, which were expanded from regenerated tissue engrafted into the D/P scaffold, as well as in human MG63 preosteoblasts. In summary, this novel CNT-based PTS approach upregulated expression of osteogenic-related genes in preosteoblasts, resulting in promotion of mineral deposition for enhanced bone repair

Introduction

Tissue engineering research in the field of regenerative medicine is currently based on three critical factors, including scaffolds, cells and growth factors[1, 2]. This therapeutic approach enables treatment and administration during the healing process. Optimal scaffolds are required for both tissue engineered constructs and for host tissues around these defects. DNA is an interesting candidate for a novel bone scaffold, because it has the great advantage of providing a phosphate group. The water solubility of DNA restricts its wider application in the biomaterials field, because of rapid elution from the implantation site within the body[3, 4]. Recently, we synthesized a novel and valuable DNA/protamine (D/P) complex scaffold (D/P scaffold), by mixing an aqueous solution of DNA (300 bps) with protamine to generate a water-insoluble white powder. The D/P scaffold has suitable viscosity for a number of clinical applications and is non-toxic with a minimal soft tissue response and antibacterial effects[5, 6]. Furthermore, we recently reported that the D/P scaffold dramatically promoted new bone regeneration in critical-sized calvarial defects (CSCDs) in rats, via osteogenesis of peripheral tissues implanted into the D/P scaffold[7-9].

It is necessary to further reduce this bone regeneration healing period, which typically takes more than 3–6 months. A reduction in healing process time usually requires mechanical stress devices, chemical cues, or laser/thermal therapies. [10, 11]. Although it remains unknown whether thermal treatment directly activates regenerative factors, hyperthermia therapy is a well-known and valuable treatment for the promotion of healing in somatic disease areas. Bone regeneration studies have previously indicated that hyperthermic stress stimulates longitudinal and concentric growth of the femur and tibia of growing rats and dogs[12-14]. However, there was no significant variation in the

growth of the lumbar or first-three caudal vertebrae, which are warmed by the animal body, regardless of the environmental conditions[12]. In contrast, hyperthermia therapy stimulates bone remodeling and the formation of new bone, thus increasing cortical bone density, suggesting an acceleration by hyperthermia in bone regeneration[11].

Carbon nanotubes (CNTs) have been considered for application in various biomedical systems, including intracellular molecular delivery and drug delivery[15, 16]. The unique properties of CNTs include their strong optical absorbance in the near-infrared (NIR) region, which enables the release of significant heat. This exothermic generation potential by NIR irradiation has been used for hyperthermia cancer therapy[17-20]. Thus, the released energy produces localized heating within a tissue, which could potentially be used for photothermal therapy in the treatment of bone defects. We therefore considered that CNT could be used as an exothermic hyperthermic device for bone repair.

The aim of the present study was to clarify whether PTS, triggered by our novel photothermal device, could enhance bone regeneration. We therefore examined the effects of PTS, on new bone deposition in the presence or absence of our osteoinductive D/P scaffold using a CSCD rat model. In addition, we examined the effects of PTS on osteoblast differentiation using D/P-cells, which were expanded from the regenerated tissue engrafted into the D/P scaffold, and MG63 preosteoblasts.

Materials and methods

Preparation of the alginate gel including carbon nanotubes (CNT-AG)

To prepare water-soluble CNTs, CNT (400 mg, single-walled type, average diameter 1 nm, average length 800 nm, CG100, South West Nanotechnology, Norman, OK) were

mixed with 300 ml of sulfuric acid and 100 ml of nitric acid, according to a previous report[21]. The resulting solid was then washed with deionized water and dried in a vacuum oven for 24 h at 80°C. Sodium alginate (2 g, Wako, Osaka, Japan) and water-soluble CNTs (10 mg) were dissolved in 100 ml of deionized water. The solution was poured into a plastic mold and then covered by a filter paper wetted with 2% calcium chloride solution for 3h to set the solution into a CNT-alginate gel (CNT-AG; 80 mm in diameter and 2mm in thickness). The CNT-AG was then carefully removed from the mold and immersed in 2% calcium chloride solution for 24h to achieve complete gel processing. The prepared CNT-AG was cut into disk-shaped specimens (10 mm diameter and 1 mm thickness). From preliminary evaluation, the CNT-AG disks showed strong heat emission by irradiating with NIR light. Because exothermic generation can be controlled by NIR irradiation conditions, the CNT-AG disk was considered a promising candidate as a photothermal device.

PTS stimulation

PTS stimulation *in vivo* and *in vitro* was carried out by irradiation of CSCDs in Sprague-Dawley (SD) rats and D/P-cells or MG63 preosteoblasts in 24-well plates, respectively. Calvarial defects, in either the presence or absence of implanted D/P disks, were also irradiated with CNT-AG (15 mm diameter) using the NIR apparatus (4.0 W/cm^2, LA-100 IR, Hayashi, Tokyo, Japan). The CNT-AG patch was set into the cranial skin and attached to the defects when rats were under deep anesthesia using isoflurane. The light tip of the NIR apparatus was located at a distance of 3 cm from the bottom of the calvarial bone and exposed to NIR light for 15 min at 42°C every day for 3 months (Figure 1A). All procedures using animals were approved by the Council on

Animal Care of Fukuoka Dental College (No.13007) and were performed in accordance with the Ethics Guidelines for Animal Experiments at Fukuoka Dental College. For *in vitro* analysis, cells in 24-well multi-plates were irradiated with CNT-AG using the NIR apparatus. The light tip of the NIR apparatus was located at a distance of 3 cm from the surface of the bottom of each well in the multi-plates (Figure 1B). Each well was exposed to NIR light for 15 min at 42°C every day for 5 consecutive days.

Preparation of DNA/protamine (D/P) complex paste disks

D/P complex paste disks were prepared as previously described (Shinozaki et. al, 2014). In brief, a solution of 300 bp fragments of sterilized salmon testis DNA was prepared and a 2% sterilized salmon testis protamine sulfate (MW = 4500) solution was provided by Maruha-Nichiro Holdings, Ltd., Tokyo, Japan. Freeze-dried D/P complex powder was kneaded in distilled water to convert it into a paste. To prepare disks of D/P complex paste, the D/P complex paste was injected into a silicone mold (internal diameter: 8 mm; height: 0.8 mm) on a polytetrafluoroethylene plate. The fabricated D/P complex disks (40 mg) were immediately and carefully removed from the polytetrafluoroethylene plate and silicone mold.

Implantation of D/P complex paste disk

Ten-week-old male SD rats (approximately weight 300 g) were used in the present study. All surgical procedures were carried out under general anesthesia induced by 2% isoflurane (Abbott Laboratories, Abbott Park, IL, USA) with an air mixture gas flow of 2.0 L/min using an anesthesia gas machine (Anesthesia machine SF-B01; MR Technology, Inc., Tsukuba, Ibaraki, Japan). After shaving the rat hair, an incision was

made in the calvariae of all rats. The skin was separated and the periosteum was exposed. The periosteum was then separated carefully from the calvarial bone. An 8-mm diameter bone defect was created in the center of the calvarial bone using an 8-mm diameter trephine bar. These procedures were carried out carefully to avoid injuring the dura. The D/P scaffold, which was prepared to 8-mm diameter, was implanted into the bone defect, and the periosteum and skin were repositioned and sutured using Vicryl 3-0 (Ethicon Inc., Somerville, NJ, USA). Empty defects were used as controls. The rats were divided into four groups: (a) blank (empty), (b) blank stimulated by PTS (c) implanted D/P (300 bp), (d) implanted D/P (300 bp) stimulated by PTS. Observation periods were carried out at 1, 2 and 3 months. Six rats were used for each group at each period.

Explanted outgrowth culture of fibrous connective tissue from calvarial defects

Fibrous connective tissue from the calvarial defects, 2 weeks after DP complex implantation, was used for the explant-outgrowth culture system. Primary cultures of mesenchymal-like cells (termed DP-cells) were harvested as outgrowths from the connective tissue explants from the calvarial defects. In brief, explants were cut into pieces of approximately 3 × 2 × 2 mm and placed on the bottoms of dishes. Explants were allowed to adhere to the dishes and were then cultured in Dulbecco's Modified Eagle's Medium (DMEM; Invitrogen, Tokyo, Japan) supplemented with 10% (v/v) fetal bovine serum (FBS; HyClone, Logan, UT, USA) and 1% (v/v) penicillin/streptomycin (PS; Invitrogen). All cultures were maintained at 37°C in a humidified incubator with 5% CO_2. After 21 days, outgrown cells from the explants were subcultured and maintained for up to an additional 7 days as secondary monolayers on tissue culture

dishes before being used for real time reverse transcription chain reaction (RT-PCR) analysis.

Cell Culture

Human MG63 preosteoblasts or DP-cells, which were derived from tissues implanted within the D/P complex in the calvarial defects, were cultured in DMEM containing 10% FBS. MG63 or DP-cells were cultured at a density of $1x10^5$ cells/ml in 24-well microplates with DMEM and 10% FBS for 1, 2, 3 and 5 days at 37°C in an atmosphere of 5% CO_2. On reaching sub-confluence, cells were cultured in DMEM with 10% FBS supplement with osteogenic induction regents, BMP-4 (10 ng/ml; PeproTech. Inc., USA) or ascorbic acid (50 μg/ml), dexamethasone (10^{-6} M) and β-glycerophosphate (10 mM). In some experiments, PTS stimulation of these cells was carried out for 15 min at 42°C every day for 5 days.

Micro-computed tomography* (μ-CT) *analysis

Micro-CT images were taken using *in vivo* μ-CT equipment (Skyscan-1176; Bruker, Belgium) at 50 kV and 500 μA. The thickness of one μ-CT slice was 35 μm. The percentage of new bone formation area in the defect was obtained from each μ-CT image and calculated as the area of newly formed bone/area of the original defect created by trephination, in accordance to our previous paper[7]. At first, the newly formed bone area on the μ-CT slice images in the horizontal direction was quantified two-dimensionally using WINROOF image analysis software (MITANI corp., Tokyo, Japan). The 8-mm diameter circles were drawn on each μ-CT slice image for analysis. A series of ten μ-CT images, showing areas of the highest amount of new bone formation,

were used for one sample analysis. The percentage of new bone formation in the defect (% of new bone) was calculated as the total area of new bone formation per 10 μ-CT slice images x100.

Histological staining

For decalcification, calvariae tissue specimens were fixed in 4% paraformaldehyde in phosphate-buffered saline (PBS), decalcified in 10% ethylenediamine tetraacetic acid (EDTA) for 4 weeks at 4°C, and then embedded in paraffin. Paraffin sections (4 μM) were then stained with H&E to visualize any histological changes. Remaining samples (used as non-decalcified specimens) were stained with Villanueva Osteochrome Bone (VOB) stain. For VOB staining, specimens were immersed in VOB solution for 3 days, dehydrated with a graded ethanol series, defatted in acetone, and then embedded in methyl methacrylate. These specimens were sectioned at 20 μm. The stained sections were observed for histology by fluorescence microscopy.

Real time Reverse Transcription-Polymerase Chain Reaction (RT-PCR)

Total RNA was isolated from MG63 preosteoblasts and DP-cells using Trizol reagent (Invitrogen, Carlsbad, CA, USA). RNA was reverse transcribed by Superscript II (Invitrogen) and amplified by Taq polymerase (Invitrogen) using gene-specific primers. The cDNA was amplified by real time RT-PCR using LightCyclerNano (Roche Diagnostics, Tokyo, Japan). Glyceraldehyde 3-phosphate dehydrogenase (GAPDH) was used as an internal control. Relative mRNA expression was normalized as the ratio of alkaline phosphatase (ALP), RUNX2, osterix (OSX) and osteocalcin (OCN) mRNAs to GAPDH expression levels. All reactions were run in hexaplicate.

Statistics

Data are expressed as means ± standard error of the mean (SEM). Differences were analyzed with one-way analysis of variance (ANOVA) and Scheffe's multiple comparison tests. *P*-values of <0.05 were considered to be significant.

Results

Micro-CT analysis

New bone regeneration was evaluated after PTS stimulation in the presence or absence of D/P scaffolds in CSCDs of 10-week-old SD rats. Although these CSCDs are previously reported not to undergo spontaneous healing 1 month after cranial surgery[22], the defects in the present study underwent some level of regeneration (22.1±2.5% of bone generation) 3 months after cranial surgery in the non-implanted CSCDs (empty; Figures 2 and 4). New bone formed in both horizontal and coronal directions. In contrast, PTS deposited new bone with small peninsulas 1 month after cranial surgery in the empty control. The PTS-induced bone deposition in CSCDs significantly increased in a time-dependent manner in the empty control up to 3 months, compared with in the absence of PTS, as shown using μ-CT and histological analysis. We recently reported that the D/P complex is a new osteoinductive scaffold suitable for calvarial defects[20]. To clarify whether PTS enhanced bone repair using the D/P scaffold, we examined the effect of PTS on bone deposition in the CSCDs following implantation of the D/P scaffold. D/P scaffold implantation alone induced large peninsulas of bone deposition compared with the blank (Figures 3 and 4). Furthermore, PTS dramatically upregulated new bone deposition in the D/P scaffold-implanted in CSCDs in a time-dependent

manner compared with the non-thermal condition.

PTS effect on histological bone healing in calvarial defects

We examined how the μ-CT images reflected the histological bone healing process in CSCDs using H&E and VOB stained sections. The main central area of the CSCD was gradually replaced with dense fibrous connective tissue (C) that contained little mineral residues. New bone (N) with C area gradually extended from the edges of these defects in a time-dependent manner (Figure 5, PTS(-) in empty). Although preexisting bone formed a lamellar structure, the new bone formed a disordered line of tissue in the calvariae. It was likely that the growth of newly formed bone on the cortical side was faster than that of the epithelial skin tissue side because the cortical side bone was longer. PTS resulted in a slight increase in N area with C area 3 months after cranial surgery. Furthermore, implantation of the D/P scaffold additionally induced new bone formation with a decrease in C area. Although D/P scaffold implantation in CSCDs upregulated new bone deposition together with some connective tissue, the PTS dramatically deposited newly formed thick lamellar bone without connective tissue, 3 months after D/P scaffold implantation (Figure 6, PTS(+) in D/P scaffold implantation). Red immunofluorescence areas were detected in the dense fibrous connective tissue of the CSCDs using VOB staining, indicating osteoid in the newly formed immature bone[23] (Figure 6, PTS (-) in empty). PTS stimulation decreased the level of red immunofluorescence, representative of immature osteoid in the bone deposition areas. D/P scaffold implantation alone also resulted in detection of a large amount of immature red staining in the bone defects. PTS stimulation with D/P scaffold implantation again reduced this (Figure 6, PTS (+) in D/P implantation). These results indicated that the

histological changes corresponded well the μ-CT data.

PTS upregulated osteogenic-related gene expression

To investigate whether PTS stimulated bone regeneration, we examined the effects of PTS on the expression of osteogenic-related genes using human MG63 preosteoblasts and DP-cells.

Incubation of MG63 cells with BMP-4 gradually induced the expression of osteogenic-related genes, including ALP, RUNX2, OSX, and OCN in a time-dependent manner (Figure 7). Osteogenic induction medium also increased expression of osteogenic-related gene in a time-dependent manner (data not shown). Furthermore, PTS significantly upregulated the expression of ALP, OSX and OCN mRNAs compared with the control without PTS. Similarly, these genes were significantly upregulated in the DP-cells in a time-dependent manner after PTS compared with the control (Figure 7).

Discussion

Efficient regeneration of bone defects is reported to be achieved using a combination of three regenerative factors: scaffolds, cells and growth factors[1, 2]. Furthermore, bone regeneration is facilitated by extracellular stimulation, such as mechanical stress devices, chemical cues, or laser/thermal therapies. In the present experiment, we used a novel photothermal device, composed of AG with CNTs and an irradiator with NIR light for hyperthermia therapy. The PTS triggered by the device upregulated bone repair with or without an osteoinductive scaffold with enhanced expression of osteogenic-related genes in MG63 preosteoblasts and DP-cells.

It has been reported that using only one heating cycle fails to elicit any significant heat shock-enhancement of osteogenesis[24]. Elevating body temperature is a common recommendation for osteoarthritic patients by taking a daily hot shower[25]. Based on this, 5 days of heating at 41–42°C was chosen to provide enough heat stimulation in our study. It has been reported that mild heat stress (39–42°C) induces osteogenesis, measured by increased ALP activity in MG63 cells[27]. The optimal temperature of 42°C also had reported to be induced heat shock promoter-mediated gene expression in NIH-3T3 cell[28]. Therefore, repetitive PTS was applied to maintain a thermal effect for 15 min at 42°C every day, to assess bone repair and osteoblast differentiation.

The response to heat stress is reported to be a protective reaction of cells to a variety of environmental and pathological stimuli[27]. The most obvious feature of the heat stress response is an increase in the synthesis of heat shock proteins (HSPs)[29, 30]. HSPs are critical components of the cells defense mechanism against injury associated with adverse stress[31, 32]. Promoters that contain heat shock elements upstream of the HSP coding region, known as heat shock promoters, can be turned on by heat shock. HSPs promote cell survival[32] and are thought to function in the protection and recovery of cells from environmental and pathological stress[29, 30]. However, little information is available on the expression of HSPs in bone remodeling. According to an immunostaining study using rat tibia, HSPs are believed to have important roles in the bone formation process, since HSP27, HSP47 and HSP70 are highly expressed in osteoblasts in newly formed bone areas[34, 35]. We found that PTS upregulated expression of osteogenic-related molecules through activation of HSP27 in MC3T3-E1 mouse osteoblasts (unpublished data). The upregulation of HSP27 in MC3T3-E1 suggests that

protection is offered from external stress, whilst also modulating several important molecules relevant to bone physiology. These results suggest that PTS may upregulated the expression of HSPs as well as osteogenic-related molecules in preosteoblasts, resulting in promotion of bone deposition in bone defects. However, the detailed mechanism of PTS-induced bone regeneration remains unclear. Further studies will address the mechanism of the PTS-activation downstream pathway into the upregulation of bone formation *in vivo* and *in vitro*.

The removable device to control multiple cell functions is an important for various biological applications, including cancer research, tissue engineering, and brain science[36, 37]. The devices of exothermic generation have been developed using UV, short-wavelength visible, and IR laser light heat to induce a thermal response. Although UV, short-wavelength visible, and IR light have poor penetration into body NIR light can penetrate at least 10 cm through deep tissue[36-38]. CNTs remarkably possess electrical, chemical, mechanical and thermal properties, indicating in useful and valuable materials in science and technology. Furthermore, CNTs include their strong optical absorbance in NIR light and release significant heat[38]. We for first time indicated that this novel device can be useful for hyperthermia in bone repair in present experiments. The device, which is composed of CNT-AG and its irradiator have the characteristics as follow; a) The CNT-AG materials can process arbitrary shape. b) The device is easy to control the setup point in temperature. c) The PTS stimulation trigged by the device has affect on the deep tissues. d) The device is convenience to move anywhere. Therefore, the device was revealed to be useful the hyperthermia therapy for bone repair as well as for cancer therapy. Furthermore, our data indicated the combination of osteoindutive D/P scaffold and PTS stimulation strongly upregulated the

bone deposition.

Hyperthermia has been used widely as a physical therapy for a number of diseases, such as inflammatory osteoarticular disorders[14] and malignant bone tumors[39, 40], as well as bone metastasis[4]. Hyperthermia therapy stimulates bone remodeling and the formation of new bone, thus increasing cortical bone density[10], suggesting that hyperthermia accelerates local bone formation. Our results taken together with those of previous reports, suggest that PTS, triggered by CNTs irradiated with NIR, not only facilitates the recovery of cells but also enhances osteogenic-related genes in MG63 preosteoblasts and DP-cells.

In summary, we found that PTS promoted bone regeneration in rat calvarial defects with or without implantation of a D/P complex osteoinductive scaffold *in vivo*. Furthermore, PTS potentially upregulated the expression of osteogenic-related genes in MG63 preosteoblasts and DP-cells. We therefore suggest that PTS may activate heat stress-dependent molecules and upregulate osteogenesis. Photothermal-induced osteogenic promotion suggests that there may be a potential use of thermotherapy for diseases characterized by bone loss, such as osteoporosis, or to accelerate fracture healing.

Acknowledgments

This work was supported by a Grant-in-Aids for Scientific Research from the Ministry of Education, Culture, Sports, Science and Technology of Japan (Nos. 24592823 and 23390455) and by a Grant-in-aid for strategic study base formation support business (S1001059) from the Japan Society for the Promotion of Science. We would like to thank Maruha-Nichiro Corporations for providing the DNA and protamine. The authors

have declared that no conflicts of interest exist.

References

1. Doll B, Sfeir C, Winn S, et al. Critical aspects of tissue-engineered therapy for bone regeneration. *Crit Rev Eukaryot Gene Expr* 2001; 11: 173-198.

2. Tabata Y. Tissue regeneration based on growth factor release. *Tissue Eng* 2003; 9 Suppl 1:S5-15.

3. Fukushima T, Ohno J, Hayakawa T, et al. Mold fabrication and biological assessment of porous DNA-chitosan complexes. *J Biomed Mater Res B Appl Biomater* 2009; 91: 746-754.

4. Fukushima T, Kawaguchi M, Hayakawa T, et al. Complexation of DNA with Cationic Polyamino Acid for Biomaterial Purposes. *J Oral Tissue Engin* 2008; 6: 24-32.

5. Fukushima T, Ohno J, Hayakawa T, et al. Polycationic protamine for water-insoluble complex formation with *DNA. Dent Mater J* 2010; 29: 529-535.

6. Mori N, Ohno J, Sakagami R, et al. Cell viabilities and biodegradation rates of DNA/protamine complexes with two different molecular weights of DNA. *J Biomed Mater Res B Appl Biomater* 2013; 101: 743-751.

7. Shinozaki Y, Yanagi T, Yamaguchi Y, et al. Osteogenic Evaluation of DNA/Protamine

Complex Paste in Rat Cranial Defects. *Journal of Hard Tissue Biology* 2013; 22: 401-408.

8. Shinozaki Y, Toda M, Ohno J, et al. Evaluation of bone formation guided by DNA/protamine complex with FGF-2 in an adult rat calvarial defect model. *J Biomed Mater Res B Appl Biomater* 2014. DOI: 10.1002/jbm.b.33143.

9. Toda M, Ohno J, Shinozaki Y, et al. Osteogenic potential for replacing cells in rat cranial defects implanted with a DNA/protamine complex paste. *Bone* 2014; 67:237-245.

10. Leon SA, Asbell SO, Arastu HH, et al. Effects of hyperthermia on bone. II. Heating of bone in vivo and stimulation of bone growth. *Int J Hyperthermia* 1993; 9: 77-87.

11. Ikenaga M, Ohura K, Kotoura Y, et al. Hyperthermic treatment of canine tibia through RF inductive heating of an intramedullary nail: a new experimental approach to hyperthermia for metastatic bone tumours. *Int J Hyperthermia* 1994; 10: 507-516.

12. Richards V and Stofer R. The stimulation of bone growth by internal heating. *Surgery* 1959; 46: 84-96.

13. Doyle JR and Smart BW. Stimulation of Bone Growth by Short-Wave Diathermy. *J*

Bone Joint Surg Am 1963; 45: 15-24.

14. Weinberger A, Abramonvici A, Fadila R, et al. The effect of local deep microwave hyperthermia on experimental zymosan-induced arthritis in rabbits. *Am J Phys Med Rehabil* 1990; 69: 239-244.

15. Dhar S, Liu Z, Thomale J, Dai H, et al. Targeted single-wall carbon nanotube-mediated Pt(IV) prodrug delivery using folate as a homing device. *J Am Chem Soc* 2008 130: 11467-11476.

16. Liu Z, Chen K, Davis C, et al. Drug delivery with carbon nanotubes for in vivo cancer treatment. *Cancer Res* 2008 68; 6652-6660.

17. O'Connell MJ, Bachilo SM, Huffman CB, et al. Band gap fluorescence from individual single-walled carbon nanotubes. *Science* 2002; 297(5581): 593-596.

18. Kam NW, O'Connell M, Wisdom JA, et al. Carbon nanotubes as multifunctional biological transporters and near-infrared agents for selective cancer cell destruction. *PNAS* 2005; 102: 11600-11605.

19. Zhou F, Xing D, Ou Z, et al. Cancer photothermal therapy in the near-infrared region by using single-walled carbon nanotubes. *J Biomed Opt* 2009; 14: 021009.

20. Ji SR, Liu C, Zhang B, et al. Carbon nanotubes in cancer diagnosis and therapy.

Biochim Biophys Acta 2010; 1806: 29-35.

21. Kawaguchi M, Fukushima T, Hayakawa T, et al. Preparation of carbon nanotube-alginate nanocomposite gel for tissue engineering. *Dent Mater J* 2006; 25: 719-725.

22. McKee MD and Nanci A. Osteopontin at mineralized tissue interfaces in bone, teeth, and osseointegrated implants: ultrastructural distribution and implications for mineralized tissue formation, turnover, and repair. *Microsc Res Tech* 1996; 33: 141-164.

23. Erlebacher A and Derynck R. Increased expression of TGF-beta 2 in osteoblasts results in an osteoporosis-like phenotype. *J Cell Biol* 1996; 132: 195-210.

24. Lim CL, Byrne C and Lee JK. Human thermoregulation and measurement of body temperature in exercise and clinical settings. *Ann Acad Med Singapore* 2008; 37: 347-353.

25. Chen J, Shi ZD, Ji X, et al. Enhanced osteogenesis of human mesenchymal stem cells by periodic heat shock in self-assembling peptide hydrogel. *Tissue Eng Part A* 2012; 19: 716-728.

26. Shui C, Scutt A. Mild heat shock induces proliferation, alkaline phosphatase activity, and mineralization in human bone marrow stromal cells and Mg-63 cells in vitro. *J*

Bone Miner Res 2001; 16: 731-741.

27. Miyako E, Deguchi T, Nakajima Y et al. Photothermal regulation of gene expression triggered by laser-induced carbon nanohorns. *PNAS* 2012; 109: 7523-7528.

28. Lindquist S, Craig EA. The heat-shock proteins. *Annu Rev Genet* 1988; 22: 631-677.

29. Schlesinger MJ. Heat shock proteins. *J Biol Chem* 1990; 265: 12111-12114.

30. Sorger PK. Heat shock factor and the heat shock response. *Cell* 1991; 65: 363-366.

31. Morimoto RI and Santoro MG. Stress-inducible responses and heat shock proteins: new pharmacologic targets for cytoprotection. *Nat Biotechnol* 1998; 16: 833-838.

32. Rylander MN1, Feng Y, Zimmermann K, et al. Measurement and mathematical modeling of thermally induced injury and heat shock protein expression kinetics in normal and cancerous prostate cells. *Int J Hyperthermia* 2010; 26: 748-764.

33. Lavoie JN, Gingras-Breton G, Tanguay RM, et al. Induction of Chinese hamster HSP27 gene expression in mouse cells confers resistance to heat shock. HSP27 stabilization of the microfilament organization. *J Biol Chem* 1993; 268: 3420-3429.

34. Tiffee JC, Griffin JP and Cooper LF. Immunolocalization of stress proteins and extracellular matrix proteins in the rat tibia. *Tissue Cell* 2000; 32: 141-147.

35. Ramos DM, Kamal F, Wimmer EA, Temporal and spatial control of transgene expression using laser induction of the hsp70 promoter. *BMC Dev Biol* 2006; 6: 55.

36. Huang H, Delikanli S, Zeng H, Remote control of ion channels and neurons through magnetic-field heating of nanoparticles. *Nat Nanotechnol* 2010; 5: 602-606.

37. König K. Multiphoton microscopy in life sciences. *J Microsc* 2000; 200: 83-104.

38. Weissleder R, Kelly K, Sun EY, et al. Cell-specific targeting of nanoparticles by multivalent attachment of small molecules. *Nat Biotechnol* 2005; 23: 1418-1423.

39. Robinson JT, Welsher K, Tabakman SM, et al. High Performance In Vivo Near-IR (>1 μm) Imaging and Photothermal Cancer Therapy with Carbon Nanotubes. *Nano Res* 2010; 3: 779-793.

40. Carter DL, MacFall JR, Clegg ST, et al. Magnetic resonance thermometry during hyperthermia for human high-grade sarcoma. *Int J Radiat Oncol Biol Phys* 1998; 40: 815-822.

Figure legends

Figure 1. Images of the experimental device arrangement for photothermal stress (PTS) stimulation under *in vivo* (A) and *in vitro* (B) conditions. The PTS device was composed of alginate gel-comprising carbon nanotubes (a: CNT-AGs) and a near-infrared ray irradiator (NIR: b). In both conditions, the top of the NIR irradiator was fixed 3 cm

distance from the CNT-AG disk. (A) *In vivo* stimulation: the CNT-AG disk (a) was placed on to the rat calvaria and irradiated 15 min at 42°C every day. (B) *In vitro* stimulation: the CNT-AG disk (a) was attached to the bottom of the multi-well plates and NIR was irradiated 15 min at 42°C every day.

Figure 2. Coronal μ-CT images of the empty control group at 1, 2 and 3 months after cranial surgery. The upper images represent un-stimulated and the lower images represent PTS-stimulated samples. The white dashed circles indicate calvarial defects just after cranial surgery (8 mm in diameter). The percentage of new bone deposition was calculated from the bony tissue in the white dashed line.

Figure 3. Coronal μ-CT images of D/P scaffold implantation at 1, 2 and 3 months after cranial surgery. The upper images represent un-stimulated and the lower images represent PTS-stimulated samples. The white dashed circles indicate calvarial defects just after cranial surgery (8 mm in diameter). The percentage of new bone deposition was calculated from the bony tissue in the white dashed line.

Figure 4. Calculated new bone deposition rate at 1, 2 and 3 months after cranial surgery.

The percentage of bone deposition was calculated from six-mice. Data shown are the mean from six mice (mean ± SEM). $^{**}P < 0.01$, un-stimulated vs. PTS-stimulated group.

Figure 5. Histological images of calvarial tissue at 3 months after cranial surgery.

B and N indicated pre-existing and new bone, respectively. C indicates connective tissues. Scale bar represents 2 mm.

Figure 6. VOB-stained section of each group of calvarial defect at 3 months after cranial surgery. The epiphysis of the regenerative bone is shown in the figure. Scale bar represents 500 μm.

Figure 7. Human MG63 preosteoblasts and DP-cells were cultured prior to performing quantitative RT-PCR for ALP, Runx2, OSX, and OCN at 0, 1, 3, and 5 days. Data shown are the mean from six mice (mean ± SEM). $^{**}P < 0.01$, un-stimulated vs. PTS-stimulated group.

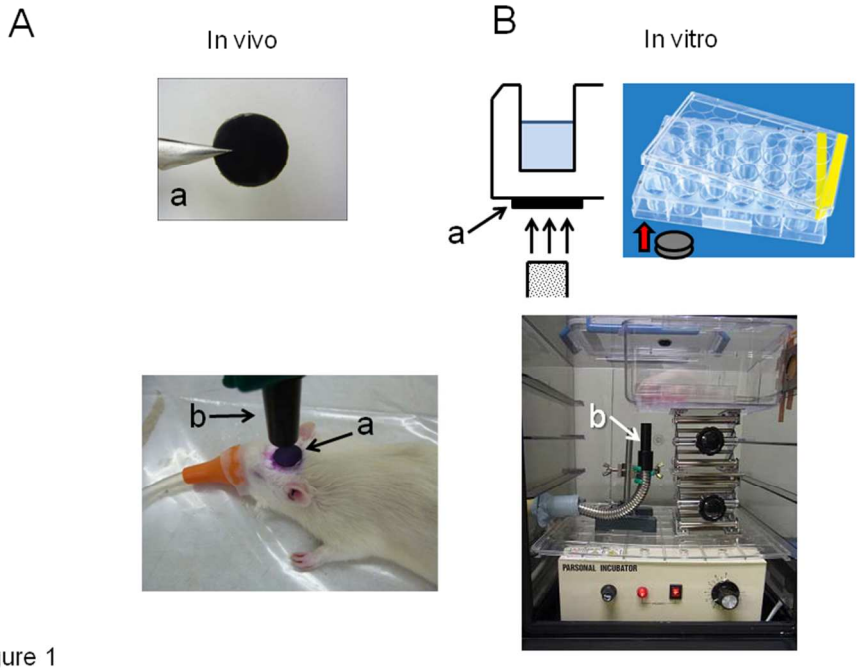

Figure 1

81x60mm (300 x 300 DPI)

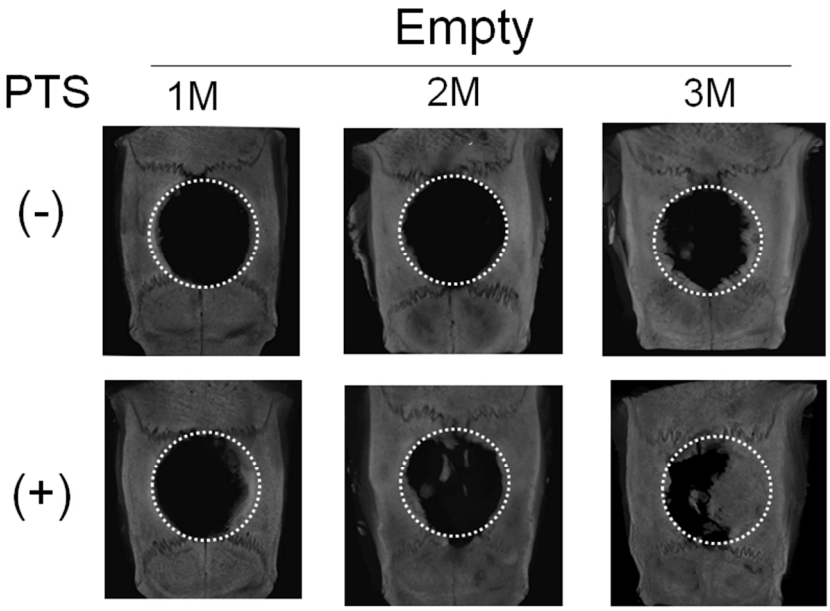

Figure 2

81x60mm (300 x 300 DPI)

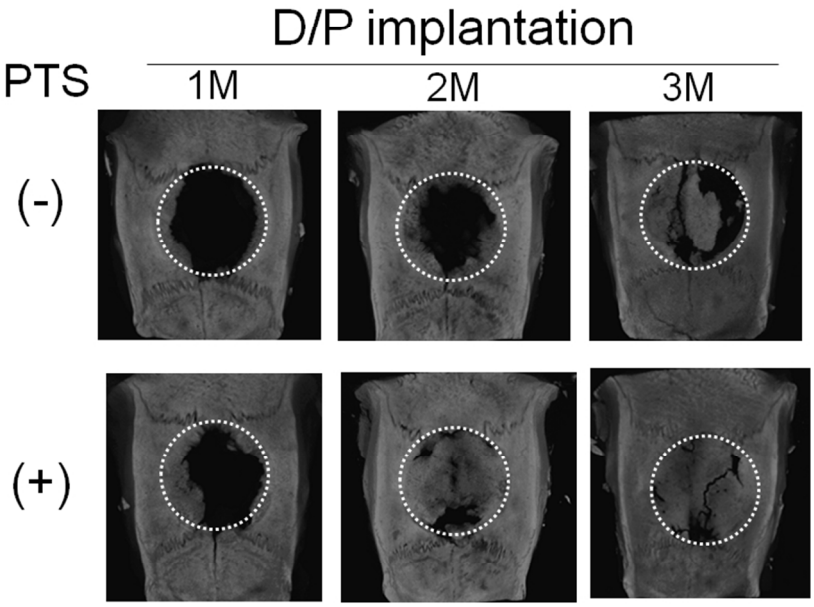

Figure 3

81x60mm (300 x 300 DPI)

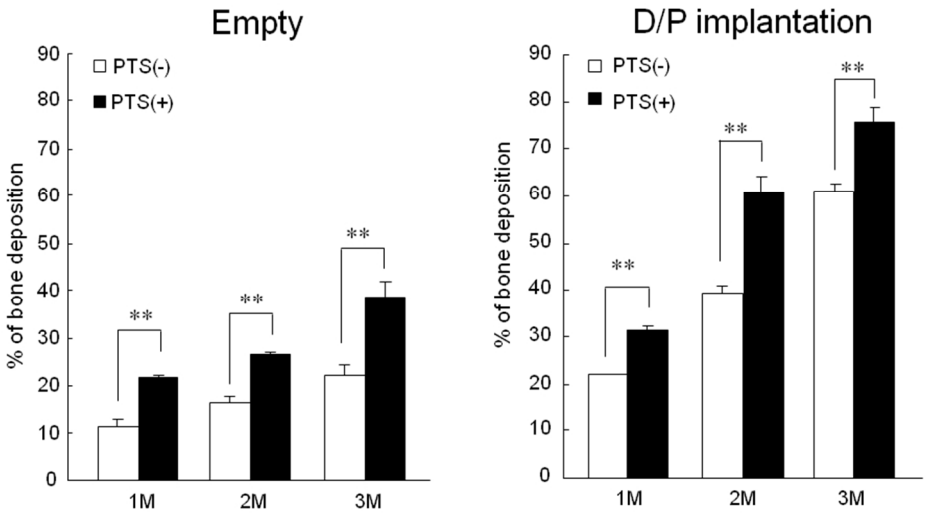

Figure 4

81x60mm (300 x 300 DPI)

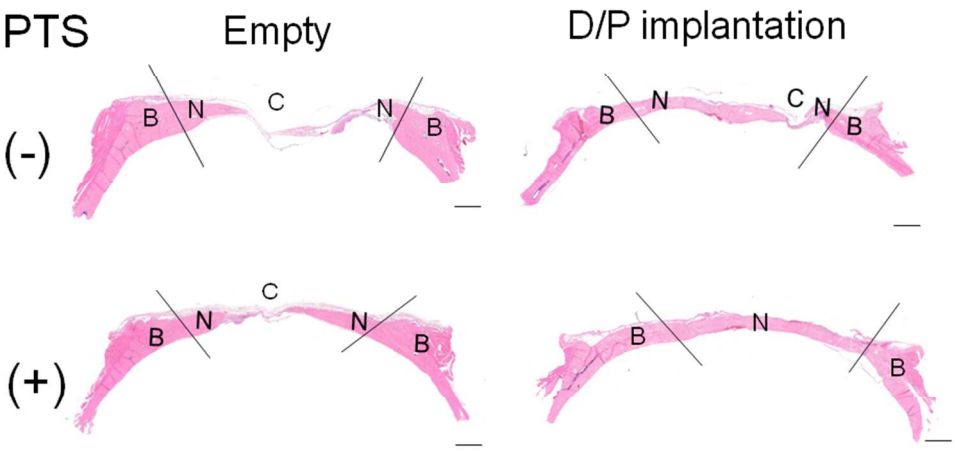

Figure 5

81x60mm (300 x 300 DPI)

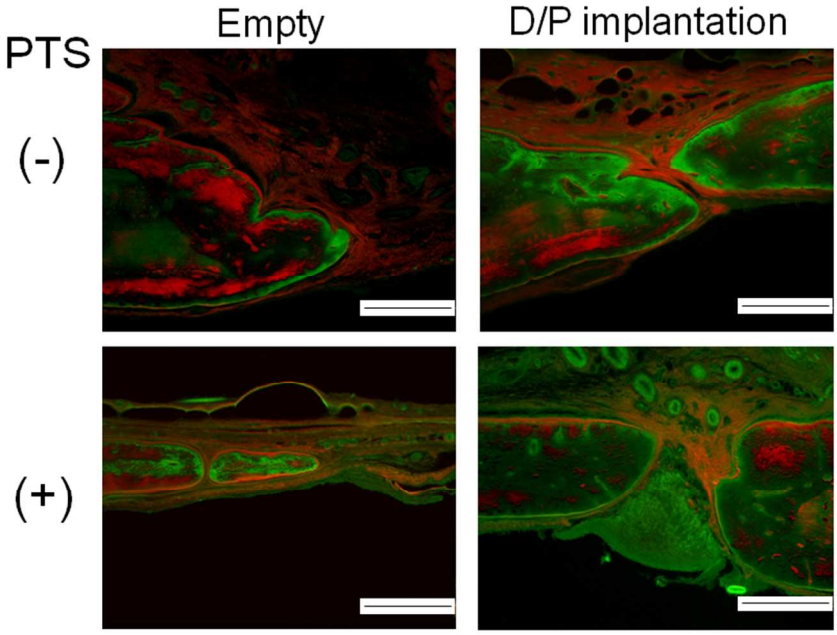

Figure 6

81x60mm (300 x 300 DPI)

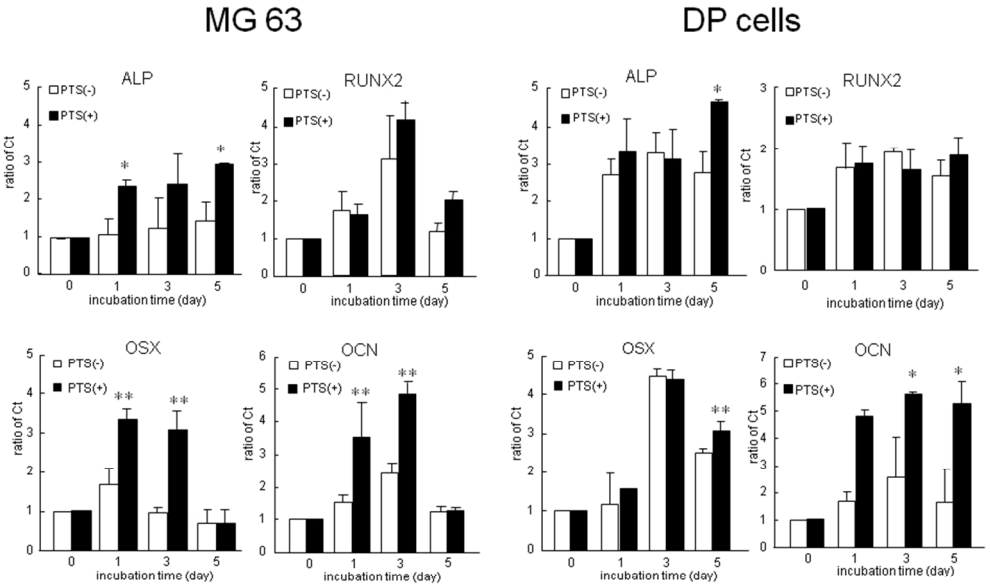

Figure 7

81x60mm (300 x 300 DPI)